NJC

PAPER

View Article Online
View Journal | View Issue

Cite this: *New J. Chem.*, 2018, **42**, 7758

Received 21st February 2018, Accepted 27th March 2018

DOI: 10.1039/c8nj00894a

rsc.li/njc

Ligand and electronic effects on copper–arylnitroso self-assembly†

F. Effaty, J. Zsombor-Pindera, A. Kazakova, B. Girard, M. S. Askari and X. Ottenwaelder *

A series of complexes were prepared by self-assembly of copper(I) precursors and arylnitroso species. The nature of the copper(I) supporting ligand (bi-, tri- or tetradentate as well as secondary *vs.* tertiary amine donors) and the electronic nature of the arylnitroso species (electron-donating or withdrawing substituents) were varied. The stoichiometry of the reaction, the topology and the electronic properties of the adducts were characterized by means of UV-vis spectroscopy, X-ray diffraction and DFT methods. The more electron-rich ligands and the more electron-poor arylnitroso species lead to an inner-sphere electron-transfer and formation of copper(II)–(arylnitrosyl radical) complexes, with a linkage topology that depends on the denticity of the supporting ligand. These results provide a canvas by which the products of similar self-assembled redox reactions can be predicted.

1. Introduction

Since the early reports on redox non-innocent ligands of aryl C-nitroso species (ArNO),[1] the interaction of nitrosoarenes with metal complexes[2] has generated considerable interest due to their implication in biological[3–6] and catalytic C–N bond formation processes.[7–9] Recent reports have highlighted the diverse redox states of ArNO ligands in metal complexes,[10–18] from ArN=O (arylnitroso) to $ArNO^{\bullet -}$ (arylnitrosyl radical) to $ArNO^{2-}$ (doubly deprotonated hydroxylamine). This series, where partners differ by $1e^-$, is isovalent‡ to the all-important O_2, $O_2^{\bullet -}$ O_2^{2-} series (O_2, superoxide and peroxide). Understanding metal–ArNO interactions will therefore provide insight into reactions involving O_2, reactive oxygen species (ROS) or into the similar HNO and NO nitric oxide chemistry.[6]

In Cu/O_2 complexes, the steric and electronic requirements of the metal and the auxiliary ligand determine the binding mode and the oxidation state of the O_2 moiety.[19,20] Since ArNO compounds are isovalent with singlet O_2, albeit less oxidizing, we have been using Cu^I precursor complexes bearing alkylamine ligands that are commonly used in Cu/O_2 chemistry.[19,20] We have previously reported the $1e^-$ and $2e^-$ reduction of nitrosoarenes by such Cu^I complexes and evidenced a controlled nitrene transfer in a C–N bond forming reaction.[13,16] These results prompted us to study the effect of systematic variations of the ligand and ArNO on the bonding geometry and the electronic state of the nitroso moiety.

In this study, we selected four ligands that differ in their denticity and/or donor atoms: a secondary diamine (DBED), a tertiary diamine (TEED), a tertiary triamine (Me_5DIEN), and a tertiary tetraamine (Me_6TREN), all based on ethylenediamine scaffolds (Scheme 1). These ligands are known to support Cu^I complexes that react with O_2 at low temperature to generate Cu_nO_2 adducts.[21–24] In addition, the reaction between $Me_6TRENCu^I$ and PhNO leads to an inner-sphere electron transfer to form a $PhNO^{\bullet -}$ radical anion that is O-bonded to a trigonal bipyramidal

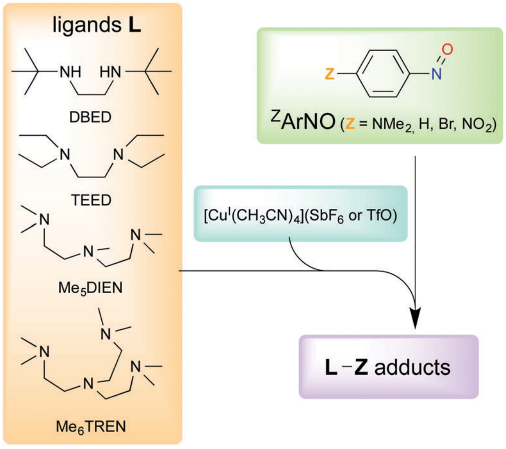

Scheme 1 General scheme for the formation of **L–Z** adducts.

Department of Chemistry and Biochemistry, Concordia University, 7141 Sherbrooke Street West, Montreal, QC, H4B 1R6, Canada. E-mail: dr.x@concordia.ca

† Electronic supplementary information (ESI) available: Selected UV-vis experiments, NMR spectra, DFT calculations. CCDC 1823004–1823010 and 1830574. For ESI and crystallographic data in CIF or other electronic format see DOI: 10.1039/c8nj00894a

‡ Strictly speaking, only HNO is isoelectronic with O_2. We use the term "isovalent" to describe the fact that ArNO species are valence-isoelectronic to O_2.

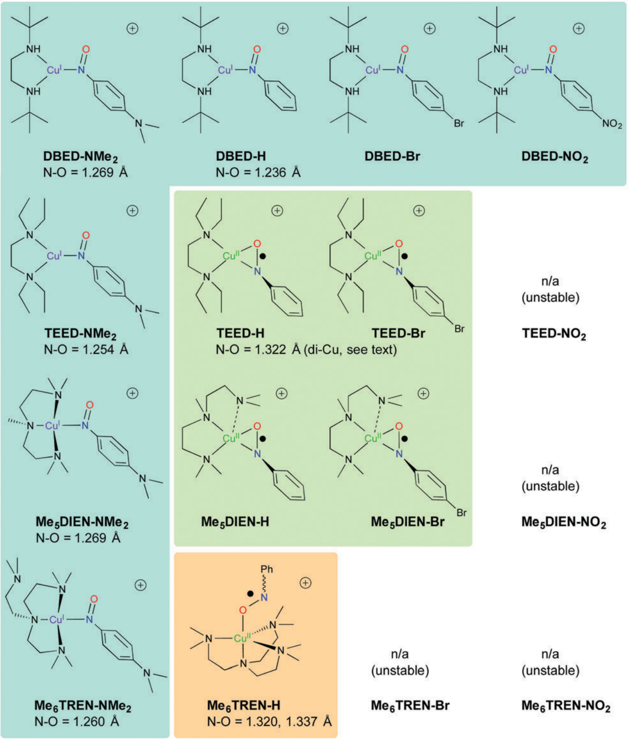

Scheme 2 Structure of the **L–Z** adducts, together with their N–O bond length characterized by crystallography (ref. 13 for **Me$_6$TREN–H**).

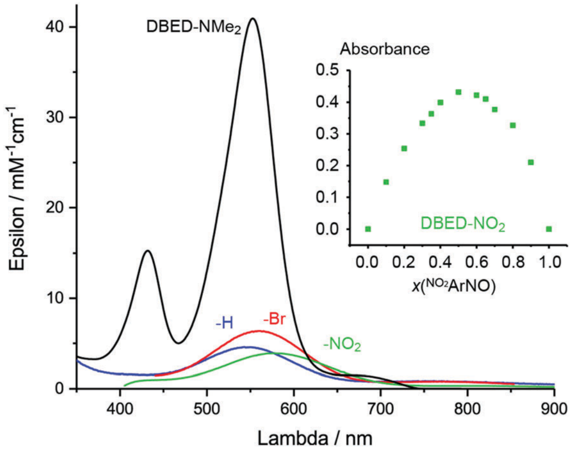

Fig. 1 UV-vis spectra of **DBED–Z** species with the Job plot for **DBED–NO$_2$**, in THF at 25 °C.

Table 1 Stoichiometric and spectroscopic data of the **L–Z** adducts[a]

		Z			
L		NMe$_2$	H	Br	NO$_2$
DBED	Model[b]	1 : 1	1 : 1	1 : 1	1 : 1
	$\log_{10} K$	4.03	4.65	4.10	3.61
	λ/nm	552	549	562	575
TEED	Model[b]	1 : 1	1 : 1/2 : 1	1 : 1	1 : 1
	$\log_{10} K$	4.06	3.94/6.03	4.07	3.72
	λ/nm	553	562	592	647
Me$_5$DIEN	Model[b]	1 : 1	1 : 1	1 : 1	1 : 1
	$\log_{10} K$	4.50	3.64	3.68	3.91
	λ/nm	545	454, 584	454,590	654
Me$_6$TREN	Model[b]	1 : 1	1 : 1		
	$\log_{10} K$	3.25	4.17	n/a	n/a
	λ/nm	551	510, 598, 942		

[a] Data obtained by fitting titration data. [b] LCu:^{Z}ArNO stoichiometry for the binding model leading to lowest residuals.

(TBP) Cu^{II}.[13] This Cu-radical complex is a structural and electronic model of the biologically relevant Me$_6$TRENCu^{II}(O$_2^{\bullet-}$) superoxide species that is only observed transiently.[24]

While being isovalent to O$_2$, ArNO species advantageously possess a synthetic handle: the aromatic ring by which their electronic properties can be systematically varied. Thus, we selected four nitrosoarene species: *p*-(dimethylamino)nitrosobenzene, nitrosobenzene, *p*-bromonitrosobenzene and *p*-nitrosonitrobenzene, herein denoted as ^{Z}ArNO (Z = NMe$_2$, H, Br and NO$_2$, Scheme 1). The adducts formed between the Cu^{I} complex of ligand L and a ^{Z}ArNO species are herein denoted as **L–Z** for simplicity. In what follows, it will be apparent that stronger donating ligands and more electron-poor ^{Z}ArNO lead to more unstable and reactive adducts, some of which could not be characterized. Notwithstanding, the comprehensive ligand and electronic variation in this family of adducts enabled us to establish bonding and electronic trends, which are summarized in Scheme 2. Highlighted in Scheme 2 are three distinct families of complexes: Cu^{I}–^{Z}ArNO species (cyan), Cu^{II} complexes with a N,O-bonded arylnitrosyl anion (green), and Cu^{II} complexes with an O-bonded arylnitrosyl anion (orange).

2. Results and discussion

2.1. Adducts with the secondary diamine ligand: DBED–Z

Reaction of [DBEDCu^{I}](X) (X^{-} = SbF$_6^{-}$ or TfO^{-}) with ^{Z}ArNO (Z = NMe$_2$, H, Br, NO$_2$) in THF led to the immediate formation of a deeply coloured purple (or red-purple for NMe$_2$) solution of **DBED–Z**. Titration of [DBEDCu^{I}]$^{+}$ with ^{Z}ArNO shows the increase of an intense absorption band around 540–590 nm with a shoulder at lower energy. Multivariate fitting of the titration data with a 1 : 1 binding model led to excellent fits, wherefrom the spectra of the adducts were extracted (Fig. 1). Binding constants (eqn (1)) extracted in this manner range between 3.6 and 4.7 log$_{10}$ units, with a net decrease on going to the more electron-poor Br and NO$_2$ arylnitroso species (Table 1). The Job plot for Z = NO$_2$ is consistent with a 1 : 1 stoichiometry (Fig. 1 inset), an important aspect to check given that a similar bidentate ligand *N*,*N*,*N*′,*N*′-tetramethylpropylenediamine (TMPD) supports a 2 : 1 adduct with ^{NO_2}ArNO, [TMPDCu^{II}(μ-η^2:η^2-^{NO_2}ArNO^{2-})Cu^{II}TMPD]$^{2+}$, in which ^{NO_2}ArNO is reduced by 2e^{-}.[16]

$$n\,\mathrm{LCu^{I}} + {}^{Z}\mathrm{ArNO} \overset{K}{\rightleftharpoons} \mathbf{L{-}Z} \tag{1}$$

The **DBED–Z** adducts are assigned as being Cu^{I}-κN-(ArN=O) species, following straightforward ligand exchange. Their ^{1}H-NMR spectra are diamagnetic (Fig. S3–S6, ESI†). Crystals suitable for X-ray diffraction were obtained for **DBED–NMe$_2$** and

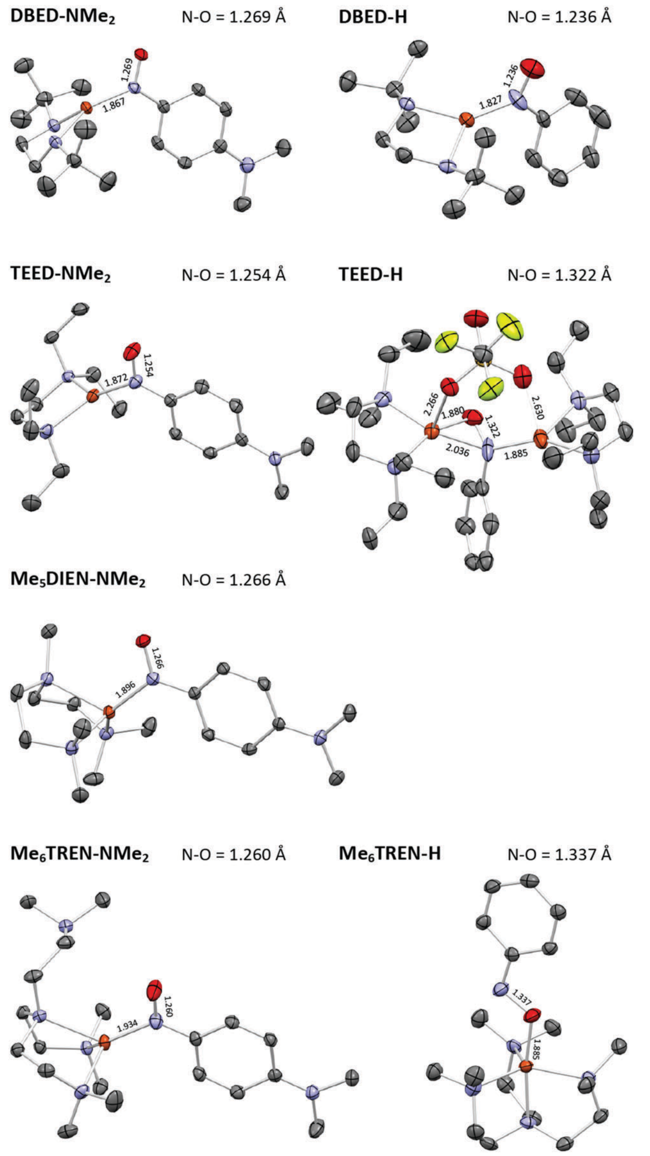

Fig. 2 ORTEP at 50% ellipsoid probability of the **L–NMe$_2$** and **L–H** adducts with main bond lengths in Å. The hydrogen atoms, counteranions and solvent molecules were removed for clarity. Structure for **Me$_6$TREN–H** (with TfO) was redrawn from ref. 13.

DBED–H with SbF_6^- counterions (Fig. 2, Table S1, ESI†).§ Both indicate a 1 : 1 complex with an N-bonded ArNO moiety where the N–O bond lengths (1.236 and 1.269 Å) are consistent with a N═O double bond character as in similar complexes.[2,8,9,14,15] Trigonal Y-shape coordination about the Cu atom, as well as Cu–N$_{DBED}$ bond lengths of 2.004–2.074 Å are consistent with a Cu^I oxidation state. The crystal structures of the more electron-poor **DBED–Br** and **DBED–NO$_2$** could not be obtained, in part because of the lower formation constants for these species and because they are less stable over long periods of time (see below). Notwithstanding, the similarity of their UV-vis spectra to that of **DBED–H** suggests the same assignment as Cu^I-κN-(ArN═O) species. Therefore, no electron transfer to the ^{Z}ArNO moiety is evident with the secondary diamine DBED ligand.

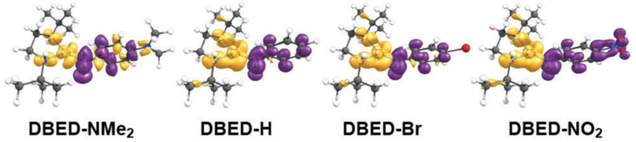

Fig. 3 TD-DFT-calculated transitions of the main component of the ≈560 nm band as electron-density difference maps, from yellow (negative density) to purple (positive density). Theoretical computations are in-line with chemical intuition: more complete MLCT upon excitation with more electron-withdrawing *para* substitution.¶

DFT calculations of the **DBED–Z** series were conducted to validate the assignment as Cu^I-κN-(ArN═O) species (ESI,† p. 9–13). In the optimized structures, the N–O bonds refine to 1.25–1.27 Å, consistent with a genuine N═O character. TD-DFT calculations reveal the presence of one major visible electronic transition systematically red-shifted from the experimental values of 549–575 nm by 44–58 nm. Orbital analysis of this transition confirms a strong metal-to-ligand charge transfer (MLCT) character that is consistent with Cu-to-ArNO backdonation. Thus, significant covalent character of the Cu–N bond and delocalization over the aromatic system explain the large intensity of these transitions. In line with the theory, increasing the electron-withdrawing character of the *para* substituent of the ArNO fragment from NMe$_2$ to NO$_2$ enhances the completeness of the MLCT (Fig. 3).

2.2. Varying the ligand in the L-NMe$_2$ series

Since electron impoverishment of the ^{Z}ArNO moiety did not induce Cu^I-to-^{Z}ArNO electron transfer in the DBED series, the second strategy employed to promote this electron transfer is to increase electron donation from the ligand. This justifies the choice of three ligands based on tertiary aliphatic amine donors: a diamine (TEED), a triamine (Me$_5$DIEN) and a tetra-amine (Me$_6$TREN). In this series of experiments, the adducts with ^{NMe2}ArNO were characterized. As in the above section, all **L-NMe$_2$** adducts have very similar UV-vis spectra and are assigned as diamagnetic 1 : 1 complexes with genuine Cu^I and ArN═O oxidation states (Fig. 4). X-ray structures were obtained for **TEED–NMe$_2$** and **Me$_5$DIEN–NMe$_2$** with SbF_6^- counterions and for **Me$_6$TREN–NMe$_2$** with TfO$^-$ counterion (Fig. 2). The N–O bond lengths in these complexes are within 1.254–1.269 Å, fully consistent with a N═O double bond character.[2,9,15] Akin to the structure of **DBED–NMe$_2$**, that of **TEED–NMe$_2$** displays a trigonal Y-shaped Cu^I geometry. The structures of **Me$_5$DIEN–NMe$_2$** and **Me$_6$TREN–NMe$_2$** are very similar, with a tetrahedral Cu^I geometry, which means that Me$_6$TREN effectively acts as a tridentate ligand in this case, with one of its $CH_2CH_2NMe_2$ arms not coordinated. This decrease in denticity is confirmed in solution, as the NMR spectrum

---

§ For crystallizations, acetonitrile from the $[Cu(CH_3CN)_4](X)$ starting material had to be removed by precipitating the complex in pentane, lest decomplexation occurred upon crystallizing, to form the starting LCu^I complex, the ^{Z}ArNO species and/or ^{Z}ArNO decomposition products.

¶ All component transitions are MLCT, except for **DBED-Br**, which has a significant LMCT contribution. See ESI,† for details.

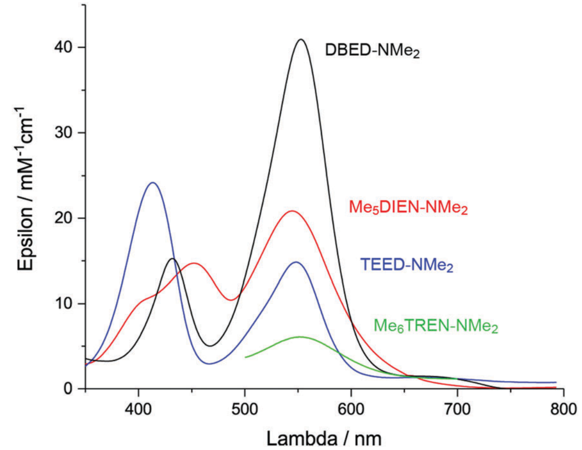

Fig. 4 UV-vis spectra of **L–NMe$_2$** species in THF at 25 °C.

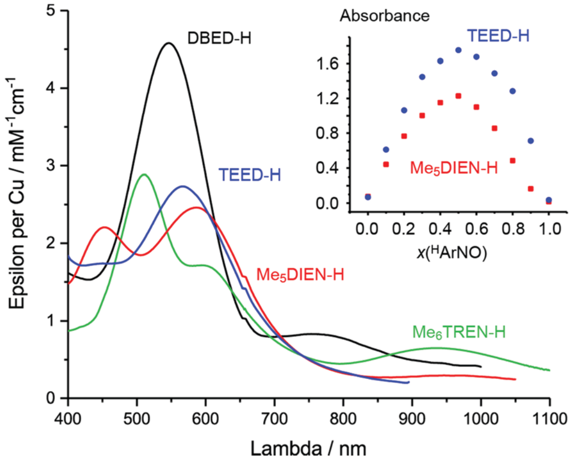

Fig. 5 UV-vis spectra of **L–H** species with Job plots for **TEED–H** and **Me$_5$DIEN–H**, in THF at 25 °C.

of **Me$_6$TREN–NMe$_2$** is fluxional (Fig. S11, ESI†). The ligand signals appear as one broad signal at 23 and 50 °C, a sign that the arms of the ligand are competing with one another for coordination.

2.3. L–H adducts with tertiary donors and electron-neutral ^{H}ArNO

The reaction of TEED-Cu^{I} with ^{H}ArNO triggers a 1e^{-} electron-transfer from the Cu^{I} to the arylnitroso moiety, which generates a Cu^{II}-(arylnitrosyl radical anion) species. The crystal structure of **TEED–H** reveals a 2:1 Cu:^{Z}ArNO complex, [TEEDCu^{II}(μ-η^{2}:η^{1}-^{H}ArNO$^{\bullet-}$)Cu^{I}TEED](TfO)$_2$, with a side-on NO moiety and a N–O bond length of 1.322 Å, consistent with a bond order of 1.5 (Fig. 2).[12] This species is similar to the one characterized by Warren *et al.* (N–O = 1.375 Å) using monoanionic β-diketiminate ligands.[11] One of the Cu centers is a square-pyramidal Cu^{II} with shorter Cu–N distances to the ligand, coordinating to both N and O of the ^{H}ArNO moiety, and a weak axial interaction with the TfO^{-} anion (Table S1, ESI†). The other Cu center is a trigonal Cu^{I}, as attested by Cu–N$_{TEED}$ distances of 2.048–2.130 Å and a negligible interaction with the O$_{PhNO}$ atom (2.666 Å) and the TfO^{-} anion (2.630 Å).

Although **TEED–H** is dinuclear in the solid state, in solution the Job plot suggests the formation of a 1:1 adduct (Fig. 5 inset). Warren showed that the LCu^{I} moiety in such dinuclear species is labile and that mononuclear [LCu^{II}(η^{2}-ArNO$^{\bullet-}$)] complexes are frequent (N–O = 1.330–1.338 Å).[11,14,25] In the case of **TEED–H**, the titration data are better fitted as a 2:1 model, although the 1:1 fit cannot be completely invalidated (Fig. S1, ESI† shows small residuals for the 1:1 model too). We construe that both 1:1 and 2:1 species can coexist in solution (Scheme 3). On going from the solution to the solid-state, the prevalent [TEEDCu^{II}(η^{2}-^{H}ArNO$^{\bullet-}$)]$^{+}$ species associates an equivalent of [TEEDCu^{I}]$^{+}$ to lead to a more stable dinuclear complex, perhaps because the TfO^{-} anion is poised to act as a bridging ligand.‖

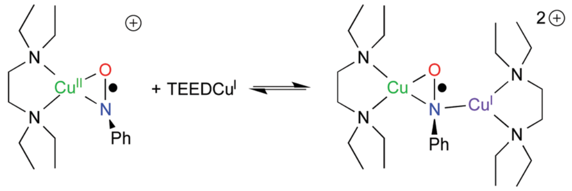

Scheme 3 Mono/dinuclear equilibrium for **TEED–H**.

The **Me$_5$DIEN–H** adduct has the same UV-vis signature as **TEED–H**, which leads us to conclude that it too has the Cu^{II}-(η^{2}-^{H}ArNO$^{\bullet-}$) formulation (Fig. 5). In solution, the titration data are better fitted as a 1:1 model (Fig. S2, ESI†), which suggests that formation of a di-Cu species does not occur, perhaps because the third amine prevents TfO^{-} binding and bridging to another Cu center. The slight asymmetry of the Job plot, however, suggests the possibility that the 2:1 adduct can exist in solution when [Me$_5$DIENCu] > [^{H}ArNO] and that other species could form at other ratios far from 1:1. Unfortunately, we were unable to crystallize this sensitive species despite using several anions, solvents and crystallization techniques.

Electron transfer occurs also in **Me$_6$TREN–H**, but the adducts adopt a very different geometry compared with bi and tridentate ligands, which translates into very different UV-vis spectra (Fig. 5).[13] In this case, Me$_6$TREN remains tetradentate, which leaves only one position open for ^{H}ArNO coordination. Thus, the ^{H}ArNO$^{\bullet-}$ anion binds *via* its O atom to the trigonal-bipyramidal Me$_6$TRENCu^{II} center. X-ray structures of this adduct depend on the anion used. With SbF$_6^{-}$, a bent Cu–O–N–Ph linkage is observed in the solid state and the solid is completely diamagnetic.** With TfO^{-}, a coplanar Cu–O–N–Ph linkage is observed in the solid state, and the solid exhibits strong ferromagnetic coupling (fits to the SQUID data suggest a triplet–singlet gap in excess of 200 cm^{-1}).[13] In solution, however, both [Me$_6$TRENCu(^{H}ArNO)](X) adducts (X^{-} = SbF$_6^{-}$ or TfO^{-}) are paramagnetic, as indicated by wide ^{1}H-NMR spectra extending

---

‖ Anecdotally, we have a case where both crystals of the mononuclear and dinuclear species are found within the same sample crystallized from a 1:1 ratio of LCu^{I} and a nitrosoarene. This will be reported at a later date.

** We also obtained the X-ray structure with BPh$_4^{-}$, where the Cu–O–N–Ph linkage is bent, but positional disorder of the Ph, N and O atoms prevents a sound structural analysis.

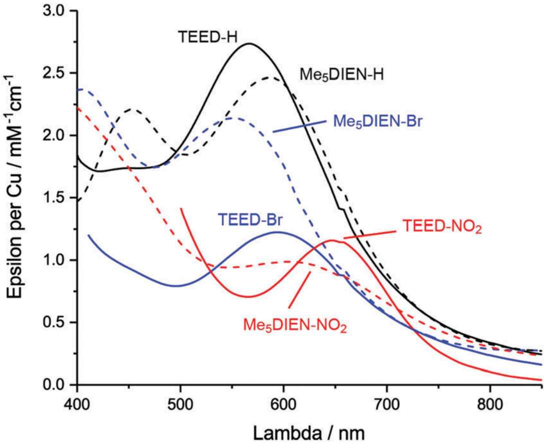

Fig. 6 UV-vis spectra of **L–Br** and **L–NO$_2$** species (L = DBED, Me$_5$DIEN) in comparison with those of **L–H** species, obtained from titrations and multivariate fitting, in THF at 25 °C. Note that the epsilons of Br and especially the NO$_2$ adducts are approximate because of the instability of the adducts.

from −33 to 20 ppm (Fig. S12, ESI†). This is consistent with a "floppy" Cu–O–N–Ph linkage in solution with an average position near Cu–O–N–Ph coplanarity. This situation would minimize the overlap between the magnetic orbitals (d_{z^2} of Cu^{II} and π of radical) and ensure a small singlet–triplet gap, which leads to a paramagnetic NMR spectrum.[26] The discrepancy between solid-state and solution structures is a testament that self-assembled structures are very sensitive to external parameters and that their geometry and electronic structure are fully subject to thermodynamic control.

2.4. Adducts with tertiary donors and electron-poor ^{Z}ArNO

Adducts with electron-poor ^{Br}ArNO and ^{NO_2}ArNO are much more reactive and unstable than **L–H** adducts and we were unable to obtain crystal structures with any of the four ligands used here. Solution studies, however, reveal a strong similarity between the UV-vis spectra of **TEED–Br** and **Me$_5$DIEN–Br** and those of **TEED–H** and **Me$_5$DIEN–H** (Fig. 6), which leads us to conclude that these adducts are side-on Cu^{II}-(^{Br}ArNO$^{\bullet-}$) species. The **TEED–NO$_2$** and **Me$_5$DIEN–NO$_2$** adducts appear to be different and could perhaps have the 2 : 1 structure of [TMPDCu^{II}(μ-η^2:η^2-^{NO_2}ArNO^{2-})Cu^{II}TMPD]$^{2+}$, with a 2e$^-$-reduced ArNO moiety.[16] Further characterization of these NO$_2$ adducts was, however, inconclusive because of their instability.

The reactivity of the **L–NO$_2$** adducts, and to a lesser extent of the **L–Br** adducts, stems from the stronger oxidizing properties of these ArNO species. When trying to crystallize **DBED–NO$_2$**, we obtained crystals of a light-red dinuclear Cu species, [DBEDCu^I(μ-η^1:η^1-DBDI)Cu^{I}DBED](SbF$_6$)$_2$, in which the bridging DBDI ligand is the diimine obtained by double oxidation of DBED, *N*,*N*′-di-*tert*-butylethane-1,2-diimine (Fig. 7a). The concomitant reduction of ^{NO_2}ArNO to hydroxylamine inevitably yields the azoxy species, ^{NO_2}Ar–N$^+$(O$^-$)=N–Ar^{NO_2}, *via* condensation.[1] These azoxy species are visible in the ^{1}H-NMR spectra of the more electron-poor adducts, in quantities that increase on going from H to Br to NO$_2$ substitution (Fig. S10, ESI†). Whether they stem from this ligand oxidation/ArNO reduction mechanism or by Cu-catalyzed decomposition of the ArNO species is yet unknown. In some **DBED–NO$_2$** and **TEED–NO$_2$** samples, we also obtained crystals of the bis-hydroxido [L$_2$Cu$_2^{II}$(μ-OH)$_2$]$^{2+}$ species (L = DBED or TEED, Fig. 7b)††.[27] These complexes are normally obtained when LCu^I reacts with O$_2$ at room temperature.[21,28] However, because the crystallizations of the **L–Z** adducts were performed under an inert atmosphere, we conclude that, like most self-assembled Cu/O$_2$ species,[20,29] **L–Z** species can become sufficiently oxidizing to abstract H atoms from the solvent, adventitious water or the ligand over several days.

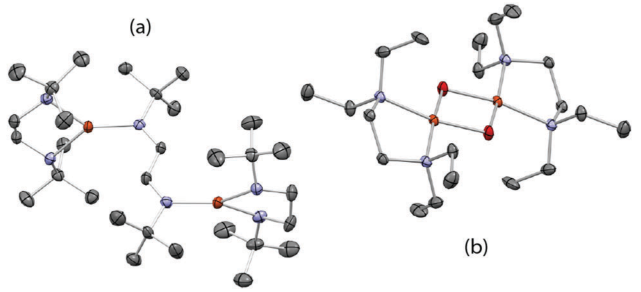

Fig. 7 ORTEP at 50% ellipsoid probability of (a) the dication in [DBED-Cu^I(μ-η^1:η^1-DBDI)Cu^{I}DBED](SbF$_6$)$_2$·THF and (b) the dication in [TEED-Cu^{II}(μ-OH)$_2$Cu^{II}TEED](SbF$_6$)$_2$·THF. The hydrogen atoms, counteranions and THF molecules were removed for clarity.

3. Conclusion

The self-assembly of arylnitroso species with Cu^I complexes is highly sensitive to the ligand denticity and electron-donating ability. Inner-sphere electron transfer is (so far) only observed with tertiary amine[13,16] or monoanionic[11,14,25] donors and requires sufficient donation from the ligand and/or electron-impoverishment of the arylnitroso moiety. The non-reduced ArNO moieties bond to Cu^I *via* their N atom exclusively, with strong backbonding into the π system of the nitroso. When inner-sphere electron transfer occurs, the d^9 ligand-field preferences of the Cu^{II} center seem to dictate the overall geometry of the adduct: square-pyramidal with bi- and tridentate ligands and trigonal-bipyramidal with C_3-symmetric tetradentate ligands. The ArNO$^{\bullet-}$ moiety adapts to these coordination requirements and adopts a side-on N,O-bonding mode with bi- and tridentate ligands *versus* an end-on O-bonding mode with tetradentate ligands. This is again proof that the ligand is paramount in controlling the self-assembly process. We also note that the weakly coordinating TfO$^-$ anion seems to be better poised to stabilize the Cu^{II} oxidation state than the virtually non-coordinating SbF$_6^-$ anion. The coordinating ability of anions was investigated in

---

[††] [(DBED)$_2$Cu$^{II}_2$(μ-OH)$_2$](PF$_6$)$_2$, obtained in an attempt to crystallize **DBED-NO$_2$**, was recognized by unit-cell comparison with the literature.[27] [(TEED)$_2$Cu$^{II}_2$(μ-OH)$_2$](SbF$_6$)$_2$·THF was determined (ESI,† CCDC 1830574) from the residue in a **TEED-NO$_2$** crystallization attempt and conforms to known structures.[37,38] The presence of these bis-hydroxido species is also suggested by weak, broad paramagnetic signals in the ^{1}H-NMR spectra of the more unstable **L-Z** adducts.

Cu/O_2 chemistry[30] and could also be a deciding factor, albeit secondary to the ligand, in the structure of the adducts. In conclusion, the present study provides a systematic canvas by which the geometric and electronic structures of other metal complexes with redox-noninnocent ArNO, O_2 or HNO moieties can be anticipated.

4. Experimental

4.1. Materials and instrumentation

Chemicals and solvents were purchased from commercial sources. Inhibitor-free solvents were dried using a MBraun SPS 800, transferred to an inert-atmosphere glovebox (MBraun Labmaster, <1 ppm of O_2 and H_2O, filled with a dry N_2 atmosphere), further degassed under vacuum, and stored over activated molecular sieves (4 Å). The ligands were distilled over CaH_2 under N_2 and stored in the glovebox. The Cu^I salts $[Cu(CH_3CN)_4](OTf)$ and $[Cu(CH_3CN)_4](SbF_6)$ were prepared by using the Kubas method,[31] recrystallized twice and stored in the glovebox. ^{H}ArNO was used as purchased and all the other ^{Z}ArNO derivatives were synthesized *via* literature procedures.[32–35] All experiments were carried out under a N_2 atmosphere, either in the glovebox or in air-tight glassware.

^{1}H-NMR spectra were recorded at 23 °C on a Varian VNMRS 500 MHz or Inova 300 MHz and referenced to internal tetramethylsilane, using samples in a 5 mm air-tight tube prepared under a N_2 atmosphere. UV-visible spectra were recorded on a B&W Tek iTrometer equipped with fiber-optic cables or an Agilent 8453 spectrophotometer. X-ray crystallographic analysis was performed using the Cu-Kα microfocus or the Mo-Kα source of a Bruker APEX-DUO diffractometer or, for **TEED–H**, the Cu-Kα enhanced source of an Oxford Diffraction Gemini A Ultra. Details regarding the crystallographic procedures are provided in the ESI† and CIFs.

4.2. Synthesis

The **L–Z** complexes were synthesized by slow addition of relevant equivalents of a ^{Z}ArNO solution to a stirring 1 : 1 solution of the Cu^I salt and ligand L in THF inside the glovebox. Crystals suitable for X-ray diffraction were grown by vapour diffusion or slow layered diffusion of pentane or diethyl ether into a THF solution of the complex at −30 °C in the glovebox. The ^{1}H-NMR spectra of the **L–Z** adducts were recorded on *in situ*-prepared L:Cu^I:^{Z}ArNO 1 : 1 : 1 mixtures in $CDCl_3$ or d^6-acetone. ^{1}H-NMR spectra of the more stable diamagnetic species: **DBED–NMe$_2$** (500 MHz, $CDCl_3$): δ 9.07 (br, 2H), 6.80 (br, 2H), 3.23 (s, 6H), 3.20 (sh, 2H), 2.93 (s, br, 4H), 1.16 (s, 18H). **DBED–H** (500 MHz, $CDCl_3$): δ 8.14 (d, 2H), 7.77 (t, 1H), 7.66 (t, 2H), 2.93 (br, 4H), 2.72 (br, 2H), 1.20 (s, 18H). **DBED–Br** (500 MHz, $CDCl_3$): δ 7.99 (d, 2H), 7.80 (d, 2H), 2.90 (s, 4H), 2.67 (s, 2H), 1.20 (s, 18H). **DBED–NO$_2$** (500 MHz, $CDCl_3$): δ 8.48 (m, 2H), 8.22 (m, 2H), 2.87 (br, 4H), 2.57 (br, 2H), 1.23 (s, 18H). **TEED–NMe$_2$** (500 MHz, $CDCl_3$): δ 8.48 (br, 2H), 6.91 (br, 2H), 3.25 (s, 6H), 2.90 (q, 8H), 2.82 (s, 4H), 1.18 (t, 12H). **TEED–H** (300 MHz, $CDCl_3$): δ 8.03 (d, 2H), 7.75 (t, 1H), 7.62 (t, 2H), 2.85 (q, 8H), 2.75 (s, 4H), 1.19 (t, 12H) **Me$_5$DIEN–NMe$_2$** (500 MHz, d^6-acetone): δ 7.98 (br, 2H), 6.95 (m, 2H), 3.27 (s, 6H), 2.85 (br, 4H), *ca.* 2.8 (sh, 3H), 2.71 (br, 4H), 2.49 (br, 12H). **Me$_5$DIEN–H** (500 MHz, d^6-acetone): δ 8.05 (m, 2H), 7.87 (m, 1H), 7.73 (m, 2H), 2.89–2.79 (multiple br, 11H), 2.59 (br, 12H). **Me$_6$TREN–NMe$_2$** (500 MHz, d^6-acetone): δ 7.95 (broad, 2H), 6.95 (broad, 2H), 3.85 (very broad, 30H), 3.28 (s, broad, 6H).

4.3. Titration and multivariate data fitting

UV-visible titrations were performed with stirring inside the glovebox or in an air-tight quartz cell prepared in the glovebox. The cell was loaded with THF, then a solution of LCu^I was added using a syringe. The titrant, ^{Z}ArNO in THF, was added by aliquots and the spectra were recorded for 30 s after each injection to allow for homogeneity. Datasets were fitted with different reasonable models using the ReactLab™ Equilibria software (Jplus Consulting) to obtain the best matching fit with minimal residuals. The stoichiometry of the complexations was evaluated using the continuous variation method, better known as the Job plot.[36]

4.4. DFT calculation methods

The theoretical electronic spectra of the four analogous **DBED–Z** adducts were predicted using TD-DFT calculations. All calculations were performed on Gaussian 09‡‡ using the GGA pure DFT functional BP86 with the triple-zeta polarized Ahlrich basis set Def2TZVP. Geometry optimizations were carried out from X-ray crystal structures using an ultrafine integration grid, tight SCF convergence criteria, and Polarized Continuum Model (PCM) solvent corrections for tetrahydrofuran (ε = 7.6). Using single-point geometries optimized under implicit solvation as input, 40 singlet excited states were calculated for each compound using TD-DFT at the same level of theory. The resulting theoretical fits of the UV-vis spectra were plotted using GaussView, with the UV-vis peak half width at the half height of 0.333 eV. Using ChemCraft, Electron Density Difference (EDD) plots were generated for each transition associated with the most intense excited state predicted in the visible range, not including de-excitation or excitation with small or negative CI expansion coefficients (see the ESI†).

Conflicts of interest

There are no conflicts to declare.

Acknowledgements

This work was funded by a Discovery Grant from NSERC (Canada), with support from the FRQNT Centre for Green Chemistry and Catalysis (Québec). We are grateful to Dr Christopher Ceccarelli from Oxford Diffraction (Varian Inc.) for data collection on **TEED–H**.

---

‡‡ Full reference in the ESI.†

References

1 P. Zuman and B. Shah, *Chem. Rev.*, 1994, **94**, 1621–1641.

2 J. Lee, L. Chen, A. H. West and G. B. Richter-Addo, *Chem. Rev.*, 2002, **102**, 1019–1066.

3 M. R. Kumar, A. Zapata, A. J. Ramirez, S. K. Bowen, W. A. Francisco and P. J. Farmer, *Proc. Natl. Acad. Sci. U. S. A.*, 2011, **108**, 18926–18931.

4 F. Doctorovich, D. E. Bikiel, J. Pellegrino, S. A. Suárez and M. A. Martí, *Acc. Chem. Res.*, 2014, **47**, 2907–2916.

5 F. Doctorovich, D. E. Bikiel, J. Pellegrino, S. A. Suárez and M. A. Martí, *Progress in Inorganic Chemistry*, John Wiley & Sons, Inc., 2014, vol. 58, pp. 145–184.

6 Z. Miao and S. B. King, *Nitric oxide*, 2016, **57**, 1–14.

7 S. Otsuka, Y. Aotani, Y. Tatsuno and T. Yoshida, *Inorg. Chem.*, 1976, **15**, 656–660.

8 R. S. Srivastava, M. A. Khan and K. M. Nicholas, *J. Am. Chem. Soc.*, 2005, **127**, 7278–7279.

9 R. S. Srivastava, N. R. Tarver and K. M. Nicholas, *J. Am. Chem. Soc.*, 2007, **129**, 15250–15258.

10 X. Dai, P. Kapoor and T. H. Warren, *J. Am. Chem. Soc.*, 2004, **126**, 4798–4799.

11 S. Wiese, P. Kapoor, K. D. Williams and T. H. Warren, *J. Am. Chem. Soc.*, 2009, **131**, 18105–18111.

12 N. C. Tomson, L. A. Labios, T. Weyhermüller, J. S. Figueroa and K. Wieghardt, *Inorg. Chem.*, 2011, **50**, 5763–5776.

13 M. S. Askari, B. Girard, M. Murugesu and X. Ottenwaelder, *Chem. Commun.*, 2011, **47**, 8055–8057.

14 K. D. Williams, A. J. P. Cardenas, J. D. Oliva and T. H. Warren, *Eur. J. Inorg. Chem.*, 2013, 3812–3816.

15 N. Xu and G. B. Richter-Addo, *Progress in Inorganic Chemistry*, John Wiley & Sons, Inc., 2014, Vol. 59, pp. 381–446.

16 M. S. Askari, M. Orio and X. Ottenwaelder, *Chem. Commun.*, 2015, **51**, 11206–11209.

17 N. C. Tomson, K. D. Williams, X. Dai, S. Sproules, S. DeBeer, T. H. Warren and K. Wieghardt, *Chem. Sci.*, 2015, **6**, 2474–2487.

18 S. Kundu, S. C. E. Stieber, M. G. Ferrier, S. A. Kozimor, J. A. Bertke and T. H. Warren, *Angew. Chem., Int. Ed.*, 2016, **55**, 10321–10325.

19 L. M. Mirica, X. Ottenwaelder and T. D. P. Stack, *Chem. Rev.*, 2004, **104**, 1013–1046.

20 C. E. Elwell, N. L. Gagnon, B. D. Neisen, D. Dhar, A. D. Spaeth, G. M. Yee and W. B. Tolman, *Chem. Rev.*, 2017, **117**, 2059–2107.

21 L. M. Mirica, D. J. Rudd, M. A. Vance, E. I. Solomon, K. O. Hodgson, B. Hedman and T. D. P. Stack, *J. Am. Chem. Soc.*, 2006, **128**, 2654–2665.

22 A. P. Cole, V. Mahadevan, L. M. Mirica, X. Ottenwaelder and T. D. P. Stack, *Inorg. Chem.*, 2005, **44**, 7345–7364.

23 S. Schindler, *Eur. J. Inorg. Chem.*, 2000, 2311–2326.

24 M. Becker, F. W. Heinemann and S. Schindler, *Chem. – Eur. J.*, 1999, **5**, 3124–3129.

25 S. Kundu, C. Greene, K. D. Williams, T. K. Salvador, J. A. Bertke, T. R. Cundari and T. H. Warren, *J. Am. Chem. Soc.*, 2017, **139**, 9112–9115.

26 P. Verma, J. Weir, L. Mirica and T. D. P. Stack, *Inorg. Chem.*, 2011, **50**, 9816–9825.

27 M. S. Askari, L. A. Rodriguez-Solano, A. Proppe, B. McAllister, J. P. Lumb and X. Ottenwaelder, *Dalton Trans.*, 2015, **44**, 12094–12097.

28 L. M. Mirica and T. D. P. Stack, *Inorg. Chem.*, 2005, **44**, 2131–2133.

29 E. A. Lewis and W. B. Tolman, *Chem. Rev.*, 2004, **104**, 1047–1076.

30 X. Ottenwaelder, D. J. Rudd, M. C. Corbett, K. O. Hodgson, B. Hedman and T. D. P. Stack, *J. Am. Chem. Soc.*, 2006, **128**, 9268–9269.

31 G. J. Kubas, *Inorg. Synth.*, 1990, **28**, 68–70.

32 A. Defoin, *Synthesis*, 2004, 706–710.

33 B. Priewisch and K. Rück-Braun, *J. Org. Chem.*, 2005, **70**, 2350–2352.

34 R. S. Heying, L. G. Nandi, A. J. Bortoluzzi and V. G. Machado, *Spectrochim. Acta, Part A*, 2015, **136**, 1491–1499.

35 G. Wu, J. Zhu, X. Mo, R. Wang and V. Terskikh, *J. Am. Chem. Soc.*, 2010, **132**, 5143–5155.

36 J. S. Renny, L. L. Tomasevich, E. H. Tallmadge and D. B. Collum, *Angew. Chem., Int. Ed.*, 2013, **52**, 11998–12013.

37 E. D. Estes, W. E. Hatfield and D. J. Hodgson, *Inorg. Chem.*, 1974, **13**, 1654–1657.

38 S. V. Pavlova, K. H. C. Chen and S. I. Chan, *Dalton Trans.*, 2004, 3261–3272.